Heliyon 6 (2020) e05360

Contents lists available at ScienceDirect

Heliyon

journal homepage: www.cell.com/heliyon

Research article

The impact of curcumin-graphene based nanoformulation on cellular interaction and redox-activated apoptosis: An *in vitro* colon cancer study

Lina A. Al-Ani [a,*], Farkaad A. Kadir [b], Najihah M. Hashim [c,d], Nurhidayatullaili M. Julkapli [a], Ali Seyfoddin [e], Jun Lu [f,g], Mohammed A. AlSaadi [a,h,i], Wageeh A. Yehye [a,**]

[a] Institute of Advanced Studies, Nanotechnology & Catalysis Research Centre (NANOCAT), University of Malaya, Kuala Lumpur, Malaysia
[b] Department of Anatomy and Medical Imaging, Faculty of Medical and Health Sciences, University of Auckland, Auckland, New Zealand
[c] Department of Pharmaceutical Chemicals, Faculty of Pharmacy, University of Malaya, Kuala Lumpur, Malaysia
[d] Centre for Natural Products and Drug Discovery (CENAR), University of Malaya, Kuala Lumpur, Malaysia
[e] Drug Delivery Research Group, Auckland University of Technology, School of Science, Auckland, New Zealand
[f] School of Science, Faculty of Health & Environmental Sciences, Auckland University of Technology. Auckland, New Zealand
[g] College of Perfume and Aroma, Shanghai Institute of Technology, Shanghai, China
[h] University of Malaya Centre for Ionic Liquids (UMCiL), University of Malaya, Kuala Lumpur, Malaysia
[i] National Chair of Materials Sciences and Metallurgy, University of Nizwa, Nizwa, Sultanate of Oman

ARTICLE INFO

Keywords:
Cancer research
Cell biology
Nanotechnology
Natural products
Anticancer
Cell membrane
Oxidative stress
Apoptosis

ABSTRACT

Natural plants derivatives have gained enormous merits in cancer therapy applications upon formulation with nanomaterials. Curcumin, as a popular research focus has acquired such improvements surpassing its disadvantageous low bioavailability. To this point, the available research data had confirmed the importance of nanomaterial type in orienting cellular response and provoking different toxicological and death mechanisms that may range from physical membrane damage to intracellular changes. This in turn underlines the poorly studied field of nanoformulation interaction with cells as the key determinant in toxicology outcomes. In this work, curcumin-AuNPs-reduced graphene oxide nanocomposite (CAG) was implemented as a model, to study the impact on cellular membrane integrity and the possible redox changes using colon cancer *in vitro* cell lines (HT-29 and SW-948), representing drug-responsive and resistant subtypes. Morphological and biochemical methods of transmission electron microscopy (TEM), apoptosis assay, reactive oxygen species (ROS) and antioxidants glutathione and superoxide dismutase (GSH and SOD) levels were examined with consideration to suitable protocols and vital optimizations. TEM micrographs proved endocytic uptake with succeeding cytoplasm deposition, which unlike other nanomaterials studied previously, conserved membrane integrity allowing intracellular cytotoxic mechanism. Apoptosis was confirmed with gold-standard morphological features observed in micrographs, while redox parameters revealed a time-dependent increase in ROS accompanied with regressive GSH and SOD levels. Collectively, this work demonstrates the success of graphene as a platform for curcumin intracellular delivery and cytotoxicity, and further highlights the importance of suitable *in vitro* methods to be used for nanomaterial validation.

1. Introduction

The solid knowledge gained through the previous decades and the ongoing research and progress in biology and technology fields had expanded the range of therapeutic strategies in use to confront cancer. Nowadays, natural product–based nanoformulations represent a promising emerging area that combines natural products' medicinal merits and nanotechnology's cancer targeting efficient drug delivery features [1]. Such multi-functional composites are needed against the aggressive nature of colon cancer, now affecting younger adults age groups with increasing incidence rates [2, 3, 4].

Natural products and specifically plant-derived agents had enormous impacts on cancer therapy research, with several compounds in use commercially as approved anti-tumour drugs [5].

* Corresponding author.
** Corresponding author.
E-mail addresses: linaalani@siswa.um.edu.my (L.A. Al-Ani), wdabdoub@um.edu.my (W.A. Yehye).

https://doi.org/10.1016/j.heliyon.2020.e05360
Received 22 June 2020; Received in revised form 3 August 2020; Accepted 23 October 2020

Recent studies had also pointed out to the increasing trend of plants use in complementary/alternative medicine (CAM) approaches, which are thought to be less toxic, more effective alternatives to conventional cancer therapies. Curcumin (CR), the polyphenolic extract of *Curcuma longa* plant, is identified as one of the most common natural products used within CAM regimes [6, 7, 8]. Its well-established safety profile, along with its multi-targeted anti--cancer activity enable selective cancer inhibition at all stages, as proven by *in vitro* and *in vivo* studies [9, 10, 11, 12]. The sum of data and literature confirm the safe well-tolerated curcumin intake for humans, even with high doses up to 12 g/day [10, 12, 13, 14]. Colon cancer particularly has gained most of CR medicinal potentials, where epidemiological data confirm the powerful relationship between CR dietary consumption and lower incidence rates [9, 10, 15]. At biochemical level, CR has also attracted much attention due to its vital role in redox reactions modulation [16, 17]. To this end, CR had shown efficiency in inducing higher ROS levels in cancer cells, which already retain a built-in elevated ROS state compared to normal counterparts [18]. The additional ROS burden can initiate oxidative stress, which in turn triggers cancer cell death [19, 20]. This mechanism, termed as ROS-modulated therapy, is now identified as the main mode-of-action (MOA) of many cancer therapeutics used today [19, 20]. Therefore, CR confers an excellent candidate to integrate with nanomaterials for a yet wider set of advantages and applications [21, 22, 23, 24, 25].

Over the years, nanoformulations have been implemented in cancer research and proven a success, especially with hydrophobic drugs sector [26, 27]. The major assets gained include cancer targeting, selective action, higher bioavailability, and most importantly, enhanced cellular uptake [28, 29, 30, 31]. The latter has now been identified as an indispensable parameter for hydrophobic drug nano-formulations [32, 33, 34, 35]. Treatment with free CR is hugely restricted by its limited aqueous solubility, poor absorption and prompt metabolism and clearance. Only around 5% of intact free CR form reaches colon area following oral intake, providing chemo-preventive action for mucosal lining [12]. On the other hand, deep colorectal tissue remains unsupplied with CR, due to low cell uptake rate [36]. Therefore, it is essential to consider cell-nanomaterials interaction when developing CR-based nanoformulations. In this regard, various nanomaterials were used previously in CR-based nanoformulation fabrication [37, 38, 39, 40, 41]. However, cell membrane interaction and uptake with the subsequent intracellular events remain poorly explored areas. Among the various nanomaterial types used in nanoformulations preparation, some were found to compromise cell membrane integrity [42, 43, 44, 45]. Graphene, and graphene based composites (GBCs), on the other hand, confer advantageous features of cellular interactions and intake, with minimal risk to cell membrane structure [33, 35, 46, 47]. In addition, the high surface area for maximal upload and biocompatibility with proper functionalization present add on merits [46, 47]. It has also been proven to be effective for hydrophobic drugs applications among different cancer types [48].

Inspired by the above, our research group has recently reported CR conjugation with graphene oxide (GO) and gold nanoparticles (AuNPs) into one nanocomposite referred as CAG [49]. The resulted novel green nanocomposite had proven dose- and time-dependent cancer cytotoxicity with preserved selectivity and safety to normal colon cell line using cellular proliferation assays, optical microscopy, and further selectivity indices calculation. These worthwhile results have motivated further elucidation of underlying mechanism of toxic actions towards colon cancer cell lines. In this work we present ultrastructural investigation of cancer cells interactions and the probable activated MOA upon treatment with CAG nanocomposite. Laboratory optimized protocols and suitable alternative assays were applied to overcome graphene-based artefacts and interferences with test probes [50]. The cumulative results in consequence prove the successful CAG uptake into colon cancer cells, and demonstrate the redox-activated apoptosis mechanism.

2. Materials and methods

2.1. Chemicals

Trypsin-EDTA solution and phosphate buffered saline were purchased from Nacalai Tesque (Kyoto, Japan). Fetal bovine serum was bought from Gibco (Maryland, USA). RPMI-1640 cell culture medium solution, Pen-Strip antibiotic (10,000 units penicillin-10 mg streptomycin/mL), reduced glutathione (GSH), L-Methionine, Ellman reagent 5, 5' Dithiobis (2-nitrobenzoic acid) (DTNB), and Nitroblue tetrazolium (NBT) were purchased from SigmaAldrich (Missouri, USA). Annexin V-FITC/propidium iodide (PI) apoptosis kit was purchased from Abcam (ab14085 kit, Abcam, Cambridge, UK). Ultrapure (UP) water (18.2 mΩ) was used throughout the experiments (Thermo Scientific, Massachusetts, USA).

2.2. CAG nanocomposite

The nanocomposite CAG was used in this study as a model for CR-graphene based nanocomposites interaction and mechanism in colon cancer cells. CAG was used in the experiments as synthesized and characterized previously [49]. Briefly, GO flakes were dispersed in de-ionized water and sonicated for 30 min in bath sonicator. The solution was then mixed with gold salt ($HAuCl_4$, Sigma-Aldrich, Missouri, USA) and heated before adding curcumin solution (1mM, Merck, Darmstadt, Germany). The reaction was sustained for 4 h, then CAG pellet was obtained through purification and freeze drying steps. Characterization data showed planar sheet morphology of rGO, with well-dispersed AuNPs on top with average AuNP size (±SEM) (15.62 ± 4.04 nm) using electron microscopy. The average hydrodynamic size of the CAG nanocomposite dispersed in cell culture media was measured using Dynamic Light Scattering (DLS) technique, recording value 171.3 ± 30.3 nm.

2.3. Cell culture

In vitro human colon cancer cell lines with diverse subtypes and distinct genetic platforms were utilized; HT-29 (colon adenocarcinoma-general good prognosis) and SW-948 (Duke's C colorectal carcinoma-poor prognosis). Cell lines were obtained from American Type Culture Collection (ATCC, Manassas, USA). Cell culture medium RPMI-1640 was used, supplemented with fetal bovine serum and Pen-Strip antibiotic at 10% and 1% (v/v), respectively, in a 37° C, 5% CO_2 incubator (Thermo Scientific, Massachusetts, USA USA).

2.4. Treatment with CAG nanocomposite

Cell lines were treated with CAG nanocomposite dispersion in RPMI-1640 media at the respective IC_{50} values that is selectively toxic to colon cancer cells, with acceptable selectivity indices (above 2.0 for both HT-29 and SW-948) towards the tested normal colon cells (CCD-841 cell line), and normal liver cells (WRL-68 cell line), as determined previously using WST-8 cellular cytotoxicity assay [49]. The following concentrations were used throughout this study (with exception to TEM studies as explained below), representing the average IC_{50} ± SEM (μg/ml) for 24, 48, and 72 h respectively; (HT-29 cell line 107.8 ± 8.9, 91.7 ± 8.0, and 59.1 ± 8.0 μg/ml), and (SW-948 cell line 100.1 ± 8.3, 94.0 ± 6.5, and 79.7 ± 14.2 μg/ml).

Alternatively, cellular TEM ultrastructure assay require the use of a safe concentration to study interaction and uptake, as reported previously [51]. Therefore, a sub-toxic CAG concentration of 50 μg/ml was implemented during TEM analysis.

2.5. Cellular ultrastructure and uptake by transmission electron microscopy imaging

To study cancer cell interaction with CAG, thin sections of cells were investigated for TEM analysis [33]. HT-29 and SW-948 cells were maintained in T75 flasks and treated with CAG for 24 h. Following that,

cells were harvested, washed with ice-cold PBS for three times, centrifuged 4000 rpm for 10 min and pre-fixed with 2.5% glutaraldehyde for 1 h at 4° C, post-fixed in 1% osmium tetroxide for 2 h. Samples were then processed with graded alcohol dehydration (35%, 50%, 70%, 90%, and 100% ethanol (v/v)). Subsequently, cell pellets were infiltrated progressively with propylene oxide: Epon at ratios 1:1 and 1:3, then with purified resin overnight. Finally, fresh resin was used for samples transfer followed by polymerization at 65 °C for 24 h. The embedded samples were cut using an ultra-microtome producing semi-this sections. Toluidine blue stain was applied later on and samples were examined by light microscope to identify regions of interest for TEM analysis. Ultra-thin sections (around 70 nm) were picked up onto 300–mesh copper grid, contrasted with uranyl acetate replacement for 5 min and lead citrate for 8 min [51, 52, 53]. Images were captured using TEM (Zeiss, LIBRA 120 model, Leipzig, Germany) using SI viewer soft imaging system.

2.6. Apoptosis studies

Cellular apoptosis upon CAG treatment was examined using both morphological and biochemical indicators. Apoptotic morphological changes were studied simultaneously in parallel with cellular uptake assay, using TEM micrographs [54].

Apoptotic biochemical event was investigated using flow cytometry Annexin V-FITC/PI assay, according to protocol supplied with kit (ab14085 kit, Abcam). In brief, colon cancer cells were seeded at 2.5×10^5 cells/ml in 6-wells plate and incubated overnight for adherence. After that, treatment with IC_{50} concentrations of CAG nanocomposite was conducted for 24 h. Standard chemotherapeutic drug 5-Fluorouracil (5-FU) served as a pro-apoptotic positive control [55]. Following drug exposure, cells were harvested, washed with ice-cold PBS before adding 500 μl binding buffer and stained with 5 μl of Annexin V-FITC, 5 μl PI at room temperature for 5 min, in dark. Samples were analysed on Flow cytometer and 10,000 events were collected for each experiment.

2.7. Reactive oxygen species (ROS) detection

To further elucidate the underlying mechanism leading to cellular death, the reactive oxygen species (ROS), generated inside cancer cells upon treatment with CAG was investigated using fluorescent assay dichlorofluorescein (DCF). Test procedure were applied as reported recently in literature [35], with additional optimization step [50]. Colon cancer cells were cultured at 3.8×10^4 cells per well in 96-well culture plates [56] and incubated overnight for attachment. The cellular treatment with CAG nanocomposite was divided into two groups in this test specifically, to indicate nanocomposite ability in inducing short-term concentration dependent and/or long term time-dependent ROS formation within cells. The first treatment group used various CAG concentrations (62.5–1000 μg/ml) for 1 h incubation, while the second treatment group included the corresponding IC_{50} values for each respective time point incubation (24, 48 and 72 h). Pre-incubated CAG with 10% FBS-supplemented-RPMI media treatment was used in this experiment as an optimization step, to overcome graphene interference and physical adsorption with fluorescent probes and its subsequent quenching action [50]. After the incubation period, cells were washed with pre-warmed PBS buffer before loading with 50μM H_2DCF-DA dye for 30 min at 37° C, 5% CO_2 incubator in dark. Subsequently, cells were washed with PBS to remove unreacted DCF probes [57], then loaded with 100μl PBS/well. Fluorescence results were recorded as intensity using microplate reader (Tecan Infinite-M200Pro, Zurich, Switzerland) at 485 nm excitation and 520 nm emission wavelengths.

2.8. Anti-oxidants levels determination

2.8.1. Cell lysis and protein levels for anti-oxidants determination

Colon cancer cell lysates were prepared as previously described [58], after treatment with CAG nanocomposite (respective IC_{50} concentration at each time point) and prior to conducting anti-oxidant GSH and SOD assays. Briefly, 1 ml of each treated cell suspension groups and control groups were centrifuged at 2500 rpm, 5 min at 4° C. Cell pellets were then washed with chilled PBS buffer, followed by incubation with 100 μL cell lysis buffer. High speed centrifugation was performed (12000 rpm, 15 min at 4° C) and cell lysates were collected and used for GSH and SOD testing, and for Bradford total protein determination as reported previously [59] for data calculation.

2.8.2. Glutathione anti-oxidant evaluation

Intracellular GSH levels were measured in response to CAG treatment using modified protocol as described in literature [60]. Calibration curve for GSH is first prepared using GSH stock standard (10 mM). Next, 50 μl cell lysate samples were added in 96-well plate. Subsequent addition of sodium phosphate reaction buffer (pH 8.0) and Ellman (DTNB) reagent were performed for each well and mixed properly. After incubation for 15 min at room temperature, results were measured immediately by microplate reader at 415 nm. Results of this assay were expressed as nmol/mg of total protein content.

2.8.3. Superoxide dismutase anti-oxidant evaluation

Enzymatic antioxidant superoxide dismutase (SOD) was measured in colon cancer cells of both control and treated groups, following Nitroblue tetrazolium (NBT) method as described by Beyer and Fridovich (1987) [61]. Briefly, superoxide anion is generated first in the sample, by mixing 1 ml of freshly prepared substrate solution (EDTA-PBS buffer, methionine, and NBT) and 20 μl of diluted cell lysate samples in glass tubs on ice. Next, SOD enzymatic activity was evaluated by measuring the extent of inhibition of superoxide anion, thus inhibition of reduction of NBT reagent, after mixing and exposure to two 18 W Sylvania lamps for 7 min. After the 7 min, the change in colour indicative for reduction of NBT in samples, was measured by microplate reader at absorbance of 560 nm. PBS-EDTA was used as blank. SOD activity in samples was calculated by the following Eqs. (1) and (2):

$$\text{Inhibition}(\%) = \frac{\text{Control Abs.} - \text{Sample Abs.}}{\text{Control Abs.}} \times 100 \quad (1)$$

$$\text{Specific activity of SOD} = \frac{\text{Enzyme unit}}{\text{Vs} \times [\text{protein}] \times \text{t}} \times \text{dilution factor} \quad (2)$$

Where;

Definition of Enzyme unit = 1 unit inhibit 50% of NBT reduction.
Vs = sample volume (0.020 ml)
[Protein] = Total Protein concentration (mg/ml)
t = time (7 min).

2.9. Statistical analysis

Data were presented as the mean ± standard error of the mean (SEM) from triplicate analysis. Statistical significance was determined using factorial analysis of variance (ANOVA) test, with p value set at < 0.05 as accepted level of significance. All analyses were performed using SPSS software (Statistical Packages for Social Science, version 22.0, IBM Corporation, NY, USA).

3. Results

3.1. Cellular interaction and uptake

Cellular interaction with nanocomposite CAG was evaluated using TEM of treated colon cancer cells. As shown in Figure 1, HT-29 cells treated with CAG clearly revealed several vesicles in the cytoplasm (Figure 1-b), compared to CAG-free cells (Figure 1-a). A magnified image of vesicles had evidently shown CAG sheets inside, without significant aggregation, proving cellular uptake of CAG sheets through endocytosis

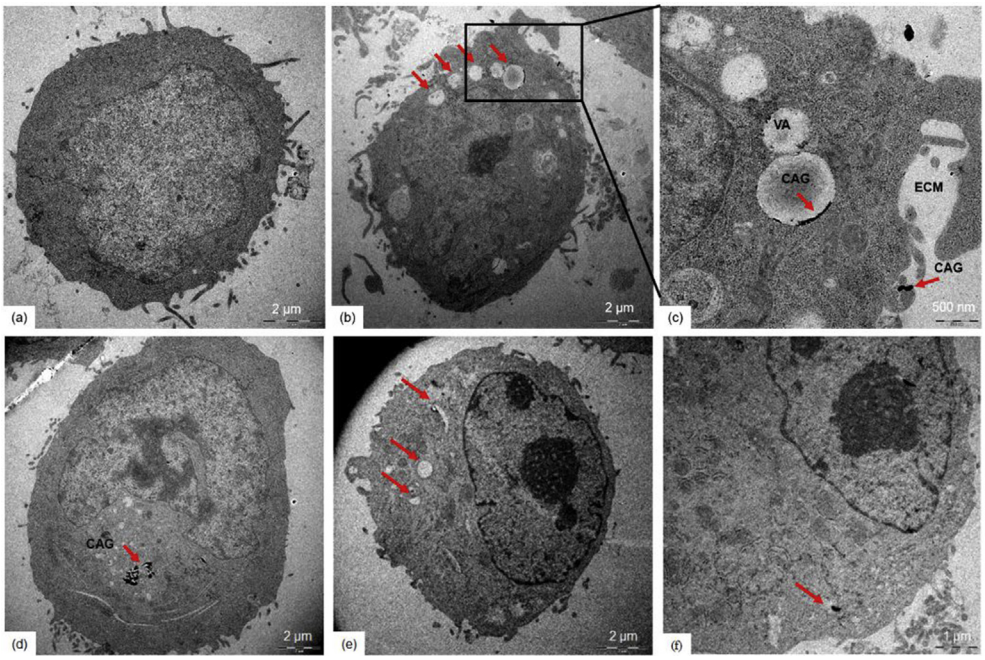

Figure 1. Cellular uptake of CAG nanocomposite. TEM micrographs of (a–d) HT-29 cell, (e–f) SW-948 cell line. Cell lines were treated with CAG nanocomposite at 50 μg/ml for 24 h. Abbreviations: CAG: nanocomposite, ECM: extracellular matrix, VA: vacuoles.

and endosome formation (Figure 1-c). The corresponding outer cell membrane after uptake showed preserved structure with no signs of mechanical damage. Furthermore, TEM micrographs have also demonstrated CAG nanocomposite located in cellular cytoplasm free from endosomal membrane surrounding (Figure 1-d). Dark areas within nucleus chromatin were also observed in CAG-up taken cells which may reflect chromatin condensation process. Similarly, the drug-resistant colon cancer subtype SW-948 exhibited an equivalent pattern proving CAG uptake intracellularly, with several vesicles (Figure 1-e), as well as free CAG located in cytoplasm (Figure 1-f).

3.2. Cellular apoptosis

For cell death type, both morphological and biochemical changes were analysed in treated cells, using TEM micrographs and Annexin V-FITC/PI assay.

Gold standard morphological changes characteristic of apoptotic cell death were observed in TEM micrographs of both cell lines HT-29 and SW-948, after CAG treatment. Figure 2-a, b, and d clearly display nucleus structural changes with chromatin condensation, accompanying cellular uptake of CAG in vesicles in both HT-29 and SW-948 cell lines, respectively. The chromatin condensation is observed clearly at the peripheral regions of nuclear membrane, along with cellular rounding and retraction of pseudopods. Subsequently, the eventual stage of apoptosis is observed with membrane blebbing forming apoptotic bodies in both colon cancer cell types (Figure 2-c and e).

Apoptotic biochemical cell membrane changes were investigated in the current work, using the standard kit protocol. Both cell lines showed no difference in fluorescence markers from control untreated cells (Supplementary Figure S1), in clear contradiction to previous morphological changes. The reasons for these results are discussed in details in discussion section.

3.3. ROS levels

The ability of CAG nanocomposite to induce oxidative stress state as a possible mechanism of action was assessed using ROS level measured with fixed short time 1 h incubation, as well as detailed 24, 48 and 72 h to observe toxicity using the toxic IC_{50} values. Fluorescent Dichloro-dihydro-fluorescein diacetate (DCFH-DA) assay with optimized method revealed increased ROS levels of HT-29 and SW-948 after only 1 h of CAG treatment (Figure 3), revealing a concentration-dependent manner. On the other hand, CAG nanocomposite treatment for 24, 48, and 72 h (Figure 4) clearly induced higher ROS levels in both cell lines, compared to control non-treated cells, suggesting a time-dependent, persistent elevated ROS levels. Collectively, the results refer to CAG nanocomposite ability to elevate cellular ROS levels in concentration and time-dependent trends.

3.4. Antioxidants GSH and SOD levels

Figure 5-a and b demonstrate the respective GSH and SOD levels in CAG treated cells versus control untreated cells. Results showed transient, mild increase in GSH levels after 24 h of CAG treatment to HT-29 and SW-948 cells, with folds increase of 1.6 and 1.2 respectively, compared to control groups. After 48 h, GSH production was only about 1.0 fold higher than control groups, whereas at longer 72 h incubation period, GSH levels recorded significant sharp decrease (2.3 folds decrease) compared to control cells.

SOD antioxidant activity in Figure 5-b displayed significant initial increase after 24 h incubation to both cell lines, followed by only modest increase at 48 h compared to control untreated groups, reaching to sharp decrease with lowest readings after 72 h.

4. Discussion

This current work represents one of the few studies focusing on cell-nanoformulation interaction with detailed microscopic record of cell uptake process, to help rule out mechanical membrane injury as a main factor in resulted cytotoxicity. The routes for nanomaterials internalization may include passive penetration or active endocytosis. Some nanomaterials, however, were reported to penetrate with strong membrane deformation and hole formation [62]. In this study, TEM micrographs revealed successful endosomal uptake of CAG nanocomposite into both HT-29 and SW-948 cell lines, without compromising membrane integrity, in agreement with previous research on GBCs treatment [46, 63, 64,

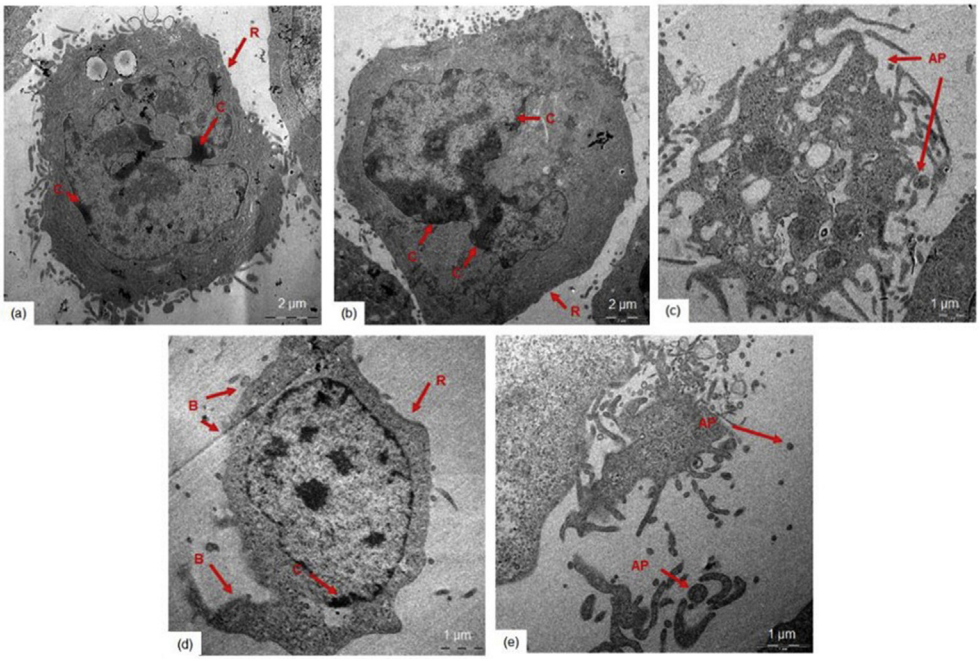

Figure 2. Apoptotic features of CAG treated cell lines. Transmission electron micrographs of (a–c) HT-29 cell, (d and e) SW-948 cell. Cell lines were treated with CAG nanocomposite at 50 μg/ml for 24 h. Abbreviations: R refers to retraction of pseudopods, C refers to chromatin condensation, B refers to membrane blebbing, AP refers to apoptotic bodies.

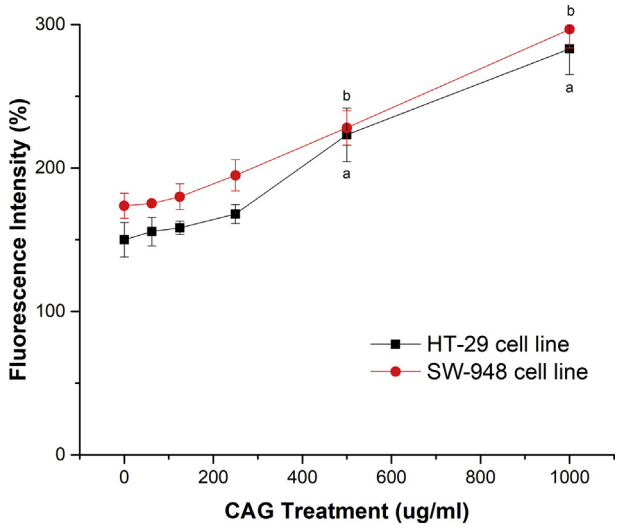

Figure 3. Formation of ROS in HT-29 and SW-948 cells upon CAG treatment for 1 h. Results are expressed as the mean ± SEM from triplicate analysis. [a] indicates significant increase in ROS production in HT-29 cell compared to control group. [b] indicates significant increase in ROS production in SW-948 cell compared to control group ($p \leq 0.05$).

65]. These results eliminate the possibility of accidental cell death (ACD) caused by instantaneous acute physical or mechanical insult to membrane [66, 67], and suggest a CAG-modulated regulated cell death (RCD) machinery. Furthermore, CAG nanocomposite detection in cytoplasm without endosomal membrane confirms the release of nanoformulation into the intracellular environment, which allows subsequent biochemical interaction and mechanisms to take place [68], surpassing the major limitation of free CR bioavailability as reported previously [36].

The next step in elucidating MOA induced by CAG nanoformulation is to investigate cell death type. Apoptosis or 'programmed/regulated cell death' resembles the preferred route for eliminating cancerous cells, while maintaining immune homeostasis and preventing pro-inflammatory reactions which can damage normal tissue surroundings [69]. Both biochemical and morphological apoptosis detection assays of CAG treated-colon cancer cells were implemented in this study. Generally, the presence of Annexin V positive results assures apoptotic biochemical cell changes [70]. However, the design of such assays that suits chemicals rather than nanomaterials [50], along with the recent toxicology reviews recommendations [71], all have indicated to rely on TEM results for apoptosis determination when using graphene-based nanomaterials.

It is only recently acknowledged that despite the superior characteristics of graphene in various applications, the same characteristics can lead to detrimental effects on the accuracy and validity of the utilized common *in vitro* toxicology assays. Graphene high surface area and charge carrier mobility represent major source of interference in fluorescence-based tests, as one example to point. The fluorescence quench effect exerted by graphene on various fluorescent probes declare fluorescence-based dyes as questionable, and call for optimization trials if quenching is reversible. In case of the common, well-established Annexin V-FITC/PI apoptosis assay, graphene controversial role and interference was only recently revealed as to exert long-distance energy transfer quenching mechanism on FITC probe [50, 72, 73]. The effect being irreversible, may lead to substantial false-negative results, as reported in literature and as tested and proved in our lab using CAG nanocomposite on colon HT-29 and SW-948 cells (Supplementary Figure S1). This highlights the importance of careful lab analysis concerning nanomaterials, and the necessity of suitable assay selection to avoid possible interference sources.

In the pursuit for alternative suitable assay that would also serve in revealing the morphological apoptotic features, TEM presents an outstanding option, acknowledged as valid apoptosis assay [54], providing unique unmatched resolution in the nano-metric size range which allows ultrastructural investigation [74]. Additionally, the precise and accurate imaging technique imposed no interference targets for graphene and GBCs. Furthermore, TEM allows recording of cellular nucleus and cytoplasm alterations, which are considered precise, accurate and specific indications for apoptosis [54, 71]. In fact, Nomenclature

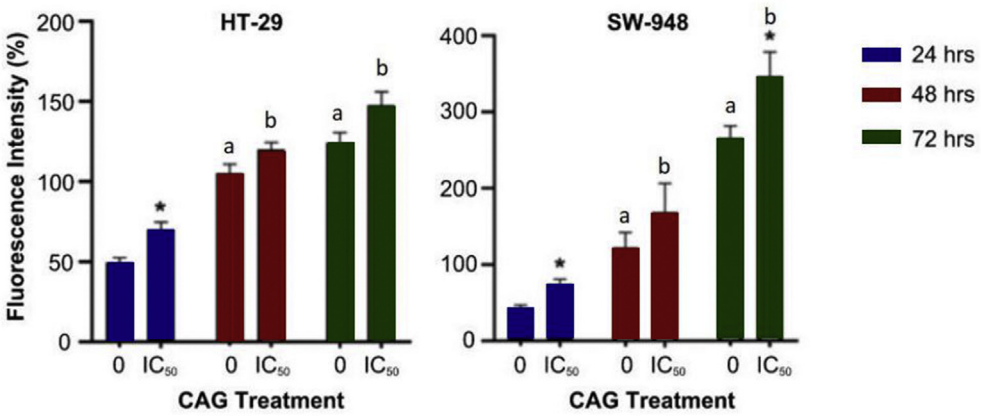

Figure 4. Formation of ROS in HT-29 and SW-948 cells upon CAG treatment. Cells received no treatment (0 control groups) or were treated with corresponding CAG nanocomposite IC_{50} value at respective time point (IC_{50} test groups). Results are expressed as the mean ± SEM from triplicate analysis. * indicates significant increase in ROS production compared to control groups ($p \leq 0.05$). [a] indicates significant difference at control groups at 48 and 72 h compared to 24 h incubation time ($p \leq 0.05$). [b] indicates significant difference at IC_{50} treatment groups at 48 and 72 h compared to 24 h incubation time ($p \leq 0.05$).

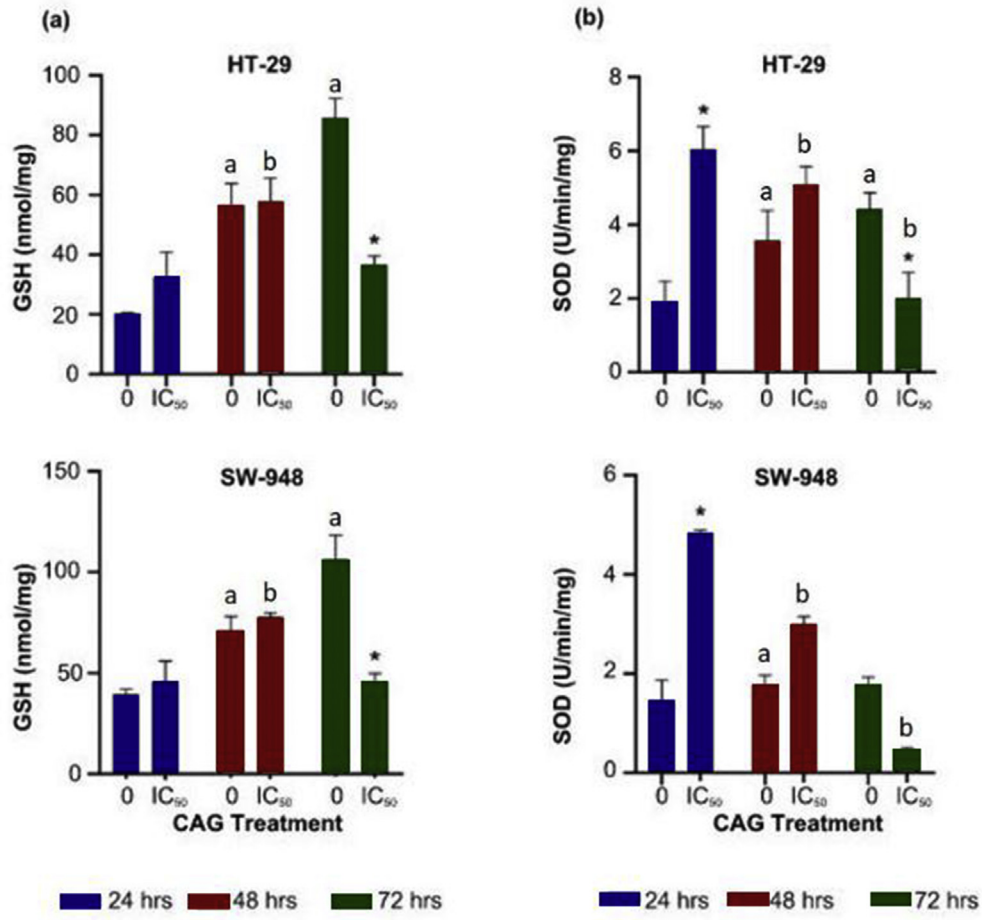

Figure 5. Anti-oxidant potentials of cells treated with CAG nanocomposite. (a) GSH levels in HT-29 and SW-948 at different time points. (b) SOD levels in HT-29 and SW-948 at different time points. Results are expressed as the mean ± SEM from triplicate analysis. * indicates significant difference compared to control groups ($p \leq 0.05$). [a] indicates significant difference at control groups at 48 and 72 h compared to 24 h incubation time ($p \leq 0.05$). [b] indicates significant difference at IC_{50} treatment groups at 48 and 72 h compared to 24 h incubation time ($p \leq 0.05$).

Committee on Cell Death (NCCD) has proposed previously that cell death identification should rely purely on morphological criteria, rather than other *in vitro* biochemical changes, to avoid non-specific conclusions [71]. This identification method is still widely used in toxicology research generally, and nanotoxicology specifically, despite the recent updated NCCD guidelines, due to various factors including nanomaterial possible interference with reagent probes [67, 75, 76]. On those grounds, we propose TEM as an effective alternative to study GBCs apoptotic effects. The multi-functionality of TEM as simultaneous qualitative detection tool for cellular uptake and apoptotic features is demonstrated in this work, saving time and resources within the process. Micrographs results as shown in Figure 2 revealed ultrastructural apoptotic hallmarks of treated colon cancer cell lines upon CAG nanocomposite uptake. These features collectively denote the gold-standard morphological attributes pertaining to apoptotic RCD death type I [53, 66, 67, 71], which further agrees with CR mechanism observed in cancer therapy [12, 77], as well as the reported triggered apoptosis by GBCs in general [78].

In between the processes of nanoformulation uptake and the eventual apoptotic cell degradation, intracellular changes and imbalances have occurred [71, 79, 80]. In this work, we have already proven CAG uptake and apoptosis induction in colon cancer cells. Yet, we are interested in the possible intermediate machinery. Depending on the drug type

applied on cancer model, speculations regarding the key trigger mechanism can be deduced and tested. CR derived redox-modulation occupies a primary role in biological, cancer-environment settings [24], and represent a common observed parameter suggesting cancer-selective pro-oxidative activity [22, 23, 25, 81, 82, 83, 84]. This event has been recognized as the principal cause for subsequent cellular imbalance, oxidative stress, disruption of numerous signalling molecules, and ultimately inducing apoptosis [24, 85]. In fact, ROS are considered accountable for possible activation and involvement in all apoptotic pathways and cascades, whether through their high-severe dose, or moderate level-prolonged effects [85].

Intracellular ROS detection was carried out using fluorescent Dichloro-dihydro-fluorescein diacetate (DCFH-DA) assay. Graphene – DCF interaction and fluorescence quench was recently studied in depth, and was explained as physical adsorption, rather than electron charge transfer. Such effect was deemed reversible, and DCF probe activity can be restored via suitable optimization, as explained earlier in methodology section [50]. Our results confirm the higher ROS levels production upon CAG treatment after 1 h incubation, which correlate with previous studies indicating prompt ROS elevation following treatment [35]. In addition, the trend was further maintained upon treatment with IC_{50} values for longer 24, 48 and 72 h incubation times. These results suggest both concentration and time-dependent, persistent oxidative stress state, and agree with CR pro-oxidant role as proved by previous reports using cancer cell models [23, 81, 82, 83]. To this point, higher baseline ROS levels were observed in the control untreated SW-948 cell line compared to HT-29 counterpart, which may indicate the cellular built-in differences in genetic platforms as reported in literature [86, 87, 88]. Interestingly, CAG nanocomposite demonstrated ability to induce ROS production in both tested cell lines which further corroborate previous findings using plant-based flavonoids [89].

For a comprehensive investigation of the cellular redox status after CAG treatment, we further assessed anti-oxidant markers levels; Glutathione (GSH) and Superoxide dismutase (SOD) [90], representing common influential antioxidant species, and the basic categories of antioxidant defence system [91]. The non-enzymatic GSH tripeptide of cysteine, glutamic acid, and glycine, effectively counteracts ROS and oxidative stress in cells, among other important functions [92, 93]. On the other hand, SOD enzyme is majorly produced by cell to reduce the superoxide anion radical. Together, they outline the primary defence lines of antioxidants [94] and confer a thorough overview on the redox state of the cell. As displayed in Figure 5, CAG incubation for shorter times resulted in mild elevation of antioxidant GSH, and a significant sharp increase in SOD activity, compared to untreated controls. However, long incubations of 72 h led to deficient GSH and SOD levels in both cell lines. The foregoing effects can be explained in stage-like chain [22, 83, 84]; the first stage where CAG treatment leads to ROS accumulation including superoxide anion inside the cell [84], followed by cellular response which calls for higher detoxification agents to regain balance [95]. In fact, the increase in anti-oxidative markers is considered as reliable indicator for accumulative ROS inside cells [95]. GSH is the most rapid and abundant anti-oxidant molecule in cells, thus it is among the first defence mechanisms induced to counteract ROS [22, 84]. In addition, SOD enzyme levels rise to sequester the elevated superoxide anion produced [84]. Despite all these efforts, the sustained elevated ROS production finally leads to GSH- and SOD-pool exhaustion, seen obviously after longer incubation times. In this case, redox balance favours pro-oxidative stress which ultimately triggers apoptosis [22, 84].

Based on the current study observations and previous reports findings [22, 83, 84], ROS-modulated apoptosis constitutes a fundamental axis in explaining the mode of action. This term might be conventional in cancer therapy methods investigated so far, however, it's astounding in the modern CR-based nano-formulations. Free CR had always suffered from poor bioavailability and low cellular uptake, diminishing its value as anti-cancer drug. Additionally, several nanomaterials failed as platforms because of their negative cellular interaction, damaging cell membrane integrity [42, 43, 44, 45]. CAG nanocomposite, in the light of the above, has successfully enabled CR uptake into cancer cells, without threatening membrane structure, enabling its crucial anti-cancer effects displayed through ROS-modulated apoptosis. These highlights encourage nanomaterials-based formulations of hydrophobic drugs, and emphasize on the suitable platforms and cellular interactions investigation.

5. Conclusion

Our data demonstrates the vital role of cell-nanoformulation interaction as a key event in confirming the subsequent biochemical toxicity mechanism. The successful cellular uptake of CAG nanocomposite into both colon cancer chemotherapy responsive and resistant-subtypes proved suitability of graphene-based composites as nanoformulation platform. Apoptotic hallmarks along with oxidative stress biomarkers complies with the well-established curcumin activity, which further proves functionality retaining upon nano-incorporation. The methods presented in this work including optimization and alternative tools highlight the importance of suitable *in vitro* assays selection and application in use with nanomaterials generally, and graphene specifically. In summary, CR-based graphene nanoformulation had advanced one step closer into achieving full understanding of mechanism, and into progress for the upcoming cancer nanotherapy.

Declarations

Author contribution statement

Lina A. Al-Ani: Conceived and designed the experiments; Performed the experiments; Analyzed and interpreted the data; Wrote the paper.

Farkaad A. Kadir, Wageeh A. Yehye: Conceived and designed the experiments; Analyzed and interpreted the data; Contributed reagents, materials, analysis tools or data; Wrote the paper.

Najihah M. Hashim, Nurhidayatullaili M. Julkapli: Contributed reagents, materials, analysis tools or data; Wrote the paper.

Ali Seyfoddin, Jun Lu, Mohammed A. AlSaadi: Analyzed and interpreted the data; Wrote the paper.

Funding statement

Wageeh Yehye was supported by Universiti Malaya Research Grant UMRG (RP044C-17AET).

Declaration of interests statement

The authors declare no conflict of interest.

Additional information

Supplementary content related to this article has been published online at https://doi.org/10.1016/j.heliyon.2020.e05360.

References

[1] D. Kashyap, H.S. Tuli, M.B. Yerer, A. Sharma, K. Sak, S. Srivastava, A. Pandey, V.K. Garg, G. Sethi, A. Bishayee, Natural Product-Based Nanoformulations for Cancer Therapy: Opportunities and Challenges, Seminars in Cancer Biology, Elsevier, 2019.

[2] A. Venugopal, E.M. Stoffel, Colorectal cancer in young Adults, Curr. Treat. Options Gastroenterol. 17 (2019) 89–98.

[3] H. Miao, J. Li, S. Hu, X. He, S.C. Partridge, J. Ren, Y. Bian, Y. Yu, B. Qiu, Long-term cognitive impairment of breast cancer patients after chemotherapy: a functional MRI study, Eur. J. Radiol. 85 (2016) 1053–1057.

[4] M. Vassilakopoulou, E. Boostandoost, G. Papaxoinis, T.d.L.M. Rouge, D. Khayat, A. Psyrri, Anticancer treatment and fertility: effect of therapeutic modalities on reproductive system and functions, Crit. Rev. Oncol.-Hematol. 97 (2016) 328–334.

[5] A.L. Demain, P. Vaishnav, Natural products for cancer chemotherapy, Microbial. Biotechnol. 4 (2011) 687–699.

[6] C. Buckner, R. Lafrenie, J. Dénommée, J. Caswell, D. Want, Complementary and alternative medicine use in patients before and after a cancer diagnosis, Curr. Oncol. 25 (2018) e275.

[7] M.A. Richardson, T. Sanders, J.L. Palmer, A. Greisinger, S.E. Singletary, Complementary/alternative medicine use in a comprehensive cancer center and the implications for oncology, J. Clin. Oncol. 18 (2000) 2505–2514.

[8] W.A. Weiger, M. Smith, H. Boon, M.A. Richardson, T.J. Kaptchuk, D.M. Eisenberg, Advising patients who seek complementary and alternative medical therapies for cancer, Ann. Intern. Med. 137 (2002) 889–903.

[9] M.C. Fadus, C. Lau, J. Bikhchandani, H.T. Lynch, Curcumin: an age-old anti-inflammatory and anti-neoplastic agent, J. Trad. Compl. Med. 7 (2017) 339–346.

[10] S.C. Gupta, S. Patchva, B.B. Aggarwal, Therapeutic roles of curcumin: lessons learned from clinical trials, AAPS J. 15 (2013) 195–218.

[11] M. López-Lázaro, Anticancer and carcinogenic properties of curcumin: considerations for its clinical development as a cancer chemopreventive and chemotherapeutic agent, Mol. Nutr. Food Res. 52 (2008) S103–S127.

[12] M. Heger, R.F. van Golen, M. Broekgaarden, M.C. Michel, The molecular basis for the pharmacokinetics and pharmacodynamics of curcumin and its metabolites in relation to cancer,, Pharmacol. Rev. 66 (2014) 222–307.

[13] S.J. Hewlings, D.S. Kalman, Curcumin: a review of its' effects on human health, Foods 6 (2017) 92.

[14] J. Epstein, I.R. Sanderson, T.T. MacDonald, Curcumin as a therapeutic agent: the evidence from in vitro, animal and human studies, Br. J. Nutr. 103 (2010) 1545–1557.

[15] K.M. Nelson, J.L. Dahlin, J. Bisson, J. Graham, G.F. Pauli, M.A. Walters, The essential medicinal chemistry of curcumin: miniperspective,, J. Med. Chem. 60 (2017) 1620–1637.

[16] T. Ak, İ. Gülçin, Antioxidant and radical scavenging properties of curcumin, Chem. Biol. Interact. 174 (2008) 27–37.

[17] S.K. Borra, P. Gurumurthy, J. Mahendra, Antioxidant and free radical scavenging activity of curcumin determined by using different in vitro and ex vivo models, J. Med. Plants Res. 7 (2013) 2680–2690.

[18] S. Sreevalsan, S. Safe, Reactive oxygen species and colorectal cancer, Curr. Colorectal Canc. Rep. 9 (2013) 350–357.

[19] C.-C. Su, J.-G. Lin, T.-M. Li, J.-G. Chung, J.-S. Yang, S.-W. Ip, W.-C. Lin, G.-W. Chen, Curcumin-induced apoptosis of human colon cancer colo 205 cells through the production of ROS, Ca2+ and the activation of caspase-3, Anticancer Res. 26 (2006) 4379–4389.

[20] L. Ou, B. Song, H. Liang, J. Liu, X. Feng, B. Deng, T. Sun, L. Shao, Toxicity of graphene-family nanoparticles: a general review of the origins and mechanisms, Part. Fibre Toxicol. 13 (2016) 57.

[21] K.E. Wong, S.C. Ngai, K.-G. Chan, L.-H. Lee, B.-H. Goh, L.-H. Chuah, Curcumin nanoformulations for colorectal cancer: a review, Front. Pharmacol. 10 (2019).

[22] C. Syng-ai, A.L. Kumari, A. Khar, Effect of curcumin on normal and tumor cells: role of glutathione and bcl-2, Mol. Canc. Therapeut. 3 (2004) 1101–1108.

[23] Y.A. Larasati, N. Yoneda-Kato, I. Nakamae, T. Yokoyama, E. Meiyanto, J.-y. Kato, Curcumin targets multiple enzymes involved in the ROS metabolic pathway to suppress tumor cell growth, Sci. Rep. 8 (2018) 2039.

[24] M.A. Khan, S. Gahlot, S. Majumdar, Oxidative stress induced by curcumin promotes the death of cutaneous T-cell lymphoma (HuT-78) by disrupting the function of several molecular targets, Mol. Canc. Therapeut. 11 (2012) 1873–1883.

[25] A. Amalraj, A. Pius, S. Gopi, S. Gopi, Biological activities of curcuminoids, other biomolecules from turmeric and their derivatives–A review, J. Trad. Compl. Med. 7 (2017) 205–233.

[26] F. Alexis, J.-W. Rhee, J.P. Richie, A.F. Radovic-Moreno, R. Langer, O.C. Farokhzad, New Frontiers in Nanotechnology for Cancer Treatment, Urologic Oncology: Seminars and Original Investigations, Elsevier, 2008, pp. 74–85.

[27] I. Brigger, C. Dubernet, P. Couvreur, Nanoparticles in cancer therapy and diagnosis, Adv. Drug Deliv. Rev. 54 (2002) 631–651.

[28] B. Haley, E. Frenkel, Nanoparticles for Drug Delivery in Cancer Treatment, Urologic Oncology: Seminars and Original Investigations, Elsevier, 2008, pp. 57–64.

[29] Z. Liu, J.T. Robinson, X. Sun, H. Dai, PEGylated nanographene oxide for delivery of water-insoluble cancer drugs, J. Am. Chem. Soc. 130 (2008) 10876–10877.

[30] R. Sinha, G.J. Kim, S. Nie, D.M. Shin, Nanotechnology in cancer therapeutics: bioconjugated nanoparticles for drug delivery, Mol. Canc. Therapeut. 5 (2006) 1909–1917.

[31] L. Brannon-Peppas, J.O. Blanchette, Nanoparticle and targeted systems for cancer therapy, Adv. Drug Deliv. Rev. 64 (2012) 206–212.

[32] S. Boonrungsiman, W. Suchaoin, P. Chetprayoon, N. Viriya-empikul, S. Aueviriyavit, R. Maniratanachote, Shape and surface properties of titanate nanomaterials influence differential cellular uptake behavior and biological responses in THP-1 cells, Biochem. Biophys. Rep. 9 (2017) 203–210.

[33] Y. Chang, S.-T. Yang, J.-H. Liu, E. Dong, Y. Wang, A. Cao, Y. Liu, H. Wang, In vitro toxicity evaluation of graphene oxide on A549 cells, Toxicol. Lett. 200 (2011) 201–210.

[34] R.-F.S. Huang, Y.-J. Wei, B.S. Inbaraj, B.-H. Chen, Inhibition of colon cancer cell growth by nanoemulsion carrying gold nanoparticles and lycopene, Int. J. Nanomed. 10 (2015) 2823.

[35] L. Horvath, A. Magrez, M. Burghard, K. Kern, L. Forro, B. Schwaller, Evaluation of the toxicity of graphene derivatives on cells of the lung luminal surface, Carbon 64 (2013) 45–60.

[36] T. Kurita, Y. Makino, Novel curcumin oral delivery systems, Anticancer Res. 33 (2013) 2807–2821.

[37] S. Mangalathillam, N.S. Rejinold, A. Nair, V.-K. Lakshmanan, S.V. Nair, R. Jayakumar, Curcumin loaded chitin nanogels for skin cancer treatment via the transdermal route, Nanoscale 4 (2012) 239–250.

[38] M. Gera, N. Sharma, M. Ghosh, D.L. Huynh, S.J. Lee, T. Min, T. Kwon, D.K. Jeong, Nanoformulations of curcumin: an emerging paradigm for improved remedial application, Oncotarget 8 (2017) 66680.

[39] M.H. Khosropanah, A. Dinarvand, A. Nezhadhosseini, A. Haghighi, S. Hashemi, F. Nirouzad, S. Khatamsaz, M. Entezari, M. Hashemi, H. Dehghani, Analysis of the antiproliferative effects of curcumin and nanocurcumin in MDA-MB231 as a breast cancer cell line, Iran. J. Pharm. Res.: IJPR 15 (2016) 231.

[40] A. Ramazani, M. Abrvash, S. Sadighian, K. Rostamizadeh, M. Fathi, Preparation and characterization of curcumin loaded gold/graphene oxide nanocomposite for potential breast cancer therapy, Res. Chem. Intermed. 44 (2018) 7891–7904.

[41] S. Malekmohammadi, H. Hadadzadeh, H. Farrokhpour, Z. Amirghofran, Immobilization of gold nanoparticles on folate-conjugated dendritic mesoporous silica-coated reduced graphene oxide nanosheets: a new nanoplatform for curcumin pH-controlled and targeted delivery, Soft Matter 14 (2018) 2400–2410.

[42] A.M. Farnoud, S. Nazemidashtarjandi, Emerging investigator series: interactions of engineered nanomaterials with the cell plasma membrane; what have we learned from membrane models? Environ. Sci.: Nano 6 (2019) 13–40.

[43] E.A. Warren, C.K. Payne, Cellular binding of nanoparticles disrupts the membrane potential, RSC Adv. 5 (2015) 13660–13666.

[44] P. Ruenraroengsak, P. Novak, D. Berhanu, A.J. Thorley, E. Valsami-Jones, J. Gorelik, Y.E. Korchev, T.D. Tetley, Respiratory epithelial cytotoxicity and membrane damage (holes) caused by amine-modified nanoparticles, Nanotoxicology 6 (2012) 94–108.

[45] J. Chen, J.A. Hessler, K. Putchakayala, B.K. Panama, D.P. Khan, S. Hong, D.G. Mullen, S.C. DiMaggio, A. Som, G.N. Tew, Cationic nanoparticles induce nanoscale disruption in living cell plasma membranes, J. Phys. Chem. B 113 (2009) 11179–11185.

[46] B. Zhang, P. Wei, Z. Zhou, T. Wei, Interactions of graphene with mammalian cells: molecular mechanisms and biomedical insights, Adv. Drug Deliv. Rev. 105 (2016) 145–162.

[47] W. Zhang, Z. Guo, D. Huang, Z. Liu, X. Guo, H. Zhong, Synergistic effect of chemo-photothermal therapy using PEGylated graphene oxide, Biomaterials 32 (2011) 8555–8561.

[48] C.-C. Liu, J.-J. Zhao, R. Zhang, H. Li, B. Chen, L.-L. Zhang, H. Yang, Multifunctionalization of graphene and graphene oxide for controlled release and targeted delivery of anticancer drugs, Am. J. Tourism Res. 9 (2017) 5197.

[49] L.A. Al-Ani, W.A. Yehye, F.A. Kadir, N.M. Hashim, M.A. AlSaadi, N.M. Julkapli, V.K. Hsiao, Hybrid nanocomposite curcumin-capped gold nanoparticle-reduced graphene oxide: anti-oxidant potency and selective cancer cytotoxicity, PloS One 14 (2019), e0216725.

[50] M.A. Creighton, J.R. Rangel-Mendez, J. Huang, A.B. Kane, R.H. Hurt, Graphene-induced adsorptive and optical artifacts during in vitro toxicology assays, Small 9 (2013) 1921–1927.

[51] X. Xie, J. Liao, X. Shao, Q. Li, Y. Lin, The effect of shape on cellular uptake of gold nanoparticles in the forms of stars, rods, and triangles,, Sci. Rep. 7 (2017) 3827.

[52] D.A. Gonzalez-Carter, B.F. Leo, P. Ruenraroengsak, S. Chen, A.E. Goode, I.G. Theodorou, K.F. Chung, R. Carzaniga, M.S. Shaffer, D.T. Dexter, Silver nanoparticles reduce brain inflammation and related neurotoxicity through induction of H 2 S-synthesizing enzymes, Sci. Rep. 7 (2017) 42871.

[53] T. Lammel, P. Boisseaux, M.-L. Fernández-Cruz, J.M. Navas, Internalization and cytotoxicity of graphene oxide and carboxyl graphene nanoplatelets in the human hepatocellular carcinoma cell line Hep G2, Part. Fibre Toxicol. 10 (2013) 27.

[54] V. Jurišić, V. Bumbaširević, In vitro assays for cell death determination, Arch. Oncol. 16 (2008) 49–54.

[55] X. Han, S. Deng, N. Wang, Y. Liu, X. Yang, Inhibitory effects and molecular mechanisms of tetrahydrocurcumin against human breast cancer MCF-7 cells, Food Nutr. Res. 60 (2016) 30616.

[56] A. Wojtala, M. Bonora, D. Malinska, P. Pinton, J. Duszynski, M.R. Wieckowski, Methods to Monitor ROS Production by Fluorescence Microscopy and Fluorometry, Methods in Enzymology, Elsevier, 2014, pp. 243–262.

[57] D. Wu, P. Yotnda, Production and detection of reactive oxygen species (ROS) in cancers, JoVE: JoVE (2011).

[58] I. Rahman, A. Kode, S.K. Biswas, Assay for quantitative determination of glutathione and glutathione disulfide levels using enzymatic recycling method, Nat. Protoc. 1 (2006) 3159–3165.

[59] N.J. Kruger, The Bradford Method for Protein Quantitation, in: J.M. Walker (Ed.), The Protein Protocols Handbook, Humana Press, Totowa, NJ, 2009, pp. 17–24.

[60] Z. Zhang, G. Xin, G. Zhou, Q. Li, V.P. Veeraraghavan, S. Krishna Mohan, D. Wang, F. Liu, Green synthesis of silver nanoparticles from Alpinia officinarum mitigates cisplatin-induced nephrotoxicity via down-regulating apoptotic pathway in rats, Artif. Cells Nanomed. Biotechnol. 47 (2019) 3212–3221.

[61] Á. Martín-Montes, B. Aguilera-Venegas, R.M. Morales-Martín, R. Martín-Escolano, S. Zamora-Ledesma, C. Marín, V.J. Arán, M. Sánchez-Moreno, In vitro assessment of 3-alkoxy-5-nitroindazole-derived ethylamines and related compounds as potential antileishmanial drugs, Bioorg. Chem. (2019) 103274.

[62] T. Wang, J. Bai, X. Jiang, G.U. Nienhaus, Cellular uptake of nanoparticles by membrane penetration: a study combining confocal microscopy with FTIR spectroelectrochemistry, ACS Nano 6 (2012) 1251–1259.

[63] M. Kucki, L. Diener, N. Bohmer, C. Hirsch, H.F. Krug, V. Palermo, P. Wick, Uptake of label-free graphene oxide by Caco-2 cells is dependent on the cell differentiation status, J. Nanobiotechnol. 15 (2017) 46.

[64] S.C. Patel, S. Lee, G. Lalwani, C. Suhrland, S.M. Chowdhury, B. Sitharaman, Graphene-based platforms for cancer therapeutics, Ther. Deliv. 7 (2016) 101–116.

[65] J. Mao, R. Guo, L.-T. Yan, Simulation and analysis of cellular internalization pathways and membrane perturbation for graphene nanosheets, Biomaterials 35 (2014) 6069–6077.

[66] L. Galluzzi, S. Aaronson, J. Abrams, E. Alnemri, D. Andrews, E. Baehrecke, N. Bazan, M. Blagosklonny, K. Blomgren, C. Borner, Guidelines for the use and interpretation of assays for monitoring cell death in higher eukaryotes, Cell Death Differ. 16 (2009) 1093.
[67] L. Galluzzi, I. Vitale, S.A. Aaronson, J.M. Abrams, D. Adam, P. Agostinis, E.S. Alnemri, L. Altucci, I. Amelio, D.W. Andrews, Molecular mechanisms of cell death: recommendations of the nomenclature committee on cell death 2018, Cell Death Differ. 25 (2018) 486.
[68] M. Bramini, S. Sacchetti, A. Armirotti, A. Rocchi, E. Vázquez, V.n. León Castellanos, T. Bandiera, F. Cesca, F. Benfenati, Graphene oxide nanosheets disrupt lipid composition, Ca2+ homeostasis, and synaptic transmission in primary cortical neurons, ACS Nano 10 (2016) 7154–7171.
[69] M.S. Ricci, W.-X. Zong, Chemotherapeutic approaches for targeting cell death pathways, Oncol. 11 (2006) 342–357.
[70] A.M. Rieger, K.L. Nelson, J.D. Konowalchuk, D.R. Barreda, Modified annexin V/propidium iodide apoptosis assay for accurate assessment of cell death, JoVE (J. Visual. Exp.) (2011), e2597.
[71] R.S. Wong, Apoptosis in cancer: from pathogenesis to treatment, J. Exp. Clin. Canc. Res. 30 (2011) 87.
[72] X. Wu, Y. Xing, K. Zeng, K. Huber, J.X. Zhao, Study of fluorescence quenching ability of graphene oxide with a layer of rigid and tunable silica spacer, Langmuir 34 (2018) 603–611.
[73] W. Lin, B. Tian, P. Zhuang, J. Yin, C. Zhang, Q. Li, T.-m. Shih, W. Cai, Graphene-based fluorescence-quenching-related fermi level elevation and electron-concentration surge, Nano Lett. 16 (2016) 5737–5741.
[74] M. Reifarth, S. Hoeppener, U.S. Schubert, Uptake and intracellular fate of engineered nanoparticles in mammalian cells: capabilities and limitations of transmission electron microscopy—polymer-based nanoparticles, Adv. Mater. 30 (2018) 1703704.
[75] A.L. Chernobrovkin, R.A. Zubarev, How well can morphology assess cell death modality? A proteomics study,, Cell Death Discov. 2 (2016) 16068.
[76] L. Galluzzi, J. Bravo-San Pedro, I. Vitale, S. Aaronson, J. Abrams, D. Adam, E. Alnemri, L. Altucci, D. Andrews, M. Annicchiarico-Petruzzelli, Essential versus accessory aspects of cell death: recommendations of the NCCD 2015, Cell Death Differ. 22 (2015) 58.
[77] A. Goel, A.B. Kunnumakkara, B.B. Aggarwal, Curcumin as "Curecumin": from kitchen to clinic, Biochem. Pharmacol. 75 (2008) 787–809.
[78] A. Piperno, A. Scala, A. Mazzaglia, G. Neri, R. Pennisi, M. Sciortino, G. Grassi, Cellular signaling pathways activated by functional graphene nanomaterials, Int. J. Mol. Sci. 19 (2018) 3365.
[79] G. Pistritto, D. Trisciuoglio, C. Ceci, A. Garufi, G. D'Orazi, Apoptosis as anticancer mechanism: function and dysfunction of its modulators and targeted therapeutic strategies, Aging (Albany NY) 8 (2016) 603.
[80] S.W. Lowe, A.W. Lin, Apoptosis in cancer, Carcinogenesis 21 (2000) 485–495.
[81] S.C. Gupta, D. Hevia, S. Patchva, B. Park, W. Koh, B.B. Aggarwal, Upsides and downsides of reactive oxygen species for cancer: the roles of reactive oxygen species in tumorigenesis, prevention, and therapy, Antioxidants Redox Signal. 16 (2012) 1295–1322.
[82] S. Majumdar, M.A. Khan, S. Gahlot, Oxidative stress induced by curcumin promotes the death of Cutaneous T cell lymphoma (HuT-78) by disrupting the function of several molecular targets, Molecular cancer therapeutics, Mol. Canc. Therapeut. (2012). 0141.2012.
[83] J. Odenthal, B.W. van Heumen, H.M. Roelofs, R.H. te Morsche, B. Marian, F.M. Nagengast, W.H. Peters, The influence of curcumin, quercetin, and eicosapentaenoic acid on the expression of phase II detoxification enzymes in the intestinal cell lines HT-29, Caco-2, HuTu 80, and LT97,, Nutr. Canc. 64 (2012) 856–863.
[84] N.M. Weir, K. Selvendiran, V.K. Kutala, L. Tong, S. Vishwanath, M. Rajaram, S. Tridandapani, S. Anant, P. Kuppusamy, Curcumin induces G2/M arrest and apoptosis in cisplatin-resistant human ovarian cancer cells by modulating Akt and p38 MAPK, Canc. Biol. Ther. 6 (2007) 178–184.
[85] M. Redza-Dutordoir, D.A. Averill-Bates, Activation of apoptosis signalling pathways by reactive oxygen species, Biochim. Biophys. Acta Mol. Cell Res. 1863 (2016) 2977–2992.
[86] K.C. Berg, P.W. Eide, I.A. Eilertsen, B. Johannessen, J. Bruun, S.A. Danielsen, M. Bjørnslett, L.A. Meza-Zepeda, M. Eknæs, G.E. Lind, Multi-omics of 34 colorectal cancer cell lines-a resource for biomedical studies, Mol. Canc. 16 (2017) 1–16.
[87] A. Sadanandam, C.A. Lyssiotis, K. Homicsko, E.A. Collisson, W.J. Gibb, S. Wullschleger, L.C.G. Ostos, W.A. Lannon, C. Grotzinger, M. Del Rio, A colorectal cancer classification system that associates cellular phenotype and responses to therapy,, Nat. Med. 19 (2013) 619–625.
[88] T. Zaidieh, J.R. Smith, K.E. Ball, Q. An, ROS as a novel indicator to predict anticancer drug efficacy, BMC Canc. 19 (2019) 1–14.
[89] N.N. Sarvestani, H. Sepehri, L. Delphi, M.M. Farimani, Eupatorin and salvigenin potentiate doxorubicin-induced apoptosis and cell cycle arrest in ht-29 and sw948 human colon cancer cells, Asian Pac. J. Cancer Prev.– APJCP 19 (2018) 131.
[90] S. Gurunathan, J.-H. Kim, Graphene oxide–silver nanoparticles nanocomposite stimulates differentiation in human neuroblastoma cancer cells (SH-SY5Y), Int. J. Mol. Sci. 18 (2017) 2549.
[91] R. Kohen, A. Nyska, Invited review: oxidation of biological systems: oxidative stress phenomena, antioxidants, redox reactions, and methods for their quantification, Toxicol. Pathol. 30 (2002) 620–650.
[92] N. Traverso, R. Ricciarelli, M. Nitti, B. Marengo, A.L. Furfaro, M.A. Pronzato, U.M. Marinari, C. Domenicotti, Role of glutathione in cancer progression and chemoresistance, Oxid. Med. Cell. Longev. 2013 (2013).
[93] H.J. Forman, Glutathione–From antioxidant to post-translational modifier, Arch. Biochem. Biophys. 595 (2016) 64–67.
[94] O. Ighodaro, O. Akinloye, First line defence antioxidants-superoxide dismutase (SOD), catalase (CAT) and glutathione peroxidase (GPX): their fundamental role in the entire antioxidant defence grid, Alexandria J. Med. 54 (2018) 287–293.
[95] M. Rawat, P. Yadukrishnan, N. Kumar, Mechanisms of action of nanoparticles in living systems, microbial biotechnology in environmental monitoring and cleanup, IGI Global (2018) 220–236.